Skyrmion-induced bound states in a superconductor

Sergey S. Pershoguba[1,3], Sho Nakosai[2,3], and Alexander V. Balatsky[1,3]
[1] *Institute for Materials Science, Los Alamos National Laboratory, Los Alamos, New Mexico 87545, USA*
[2] *Condensed Matter Theory Laboratory, RIKEN, Wako, Saitama, 351-0198, Japan and*
[3] *Nordita, Center for Quantum Materials, KTH Royal Institute of Technology, and Stockholm University, Roslagstullsbacken 23, S-106 91 Stockholm, Sweden*

(Dated: April 1, 2016)

We consider a superconductor proximity coupled to a two-dimensional ferromagnetic film with a skyrmion texture. Using the T-matrix calculations and numerical modeling we calculate the spin-polarized local density of states in the superconductor in the vicinity of the skyrmion. We predict the skyrmion bound states (SBS) that are induced in the superconductor, similar to the well-known Yu-Shiba-Rusinov (YSR) states. The SBS wavefunctions have spatial power-law decay. Presence of the SBS suggests the mechanism by which superconductivity could facilitate an effective long-range interaction between skyrmions when their SBS wavefunctions overlap.

PACS numbers: 12.39.Dc, 74.45.+c

Introduction.— Skyrmions, topological particle-like configurations of a continuous vector field, were originally proposed in the context of high-energy physics [1]. Nevertheless, it was suggested theoretically [2, 3] and recently confirmed experimentally [4–8] that skyrmions exist in chiral ferromagnets in the presence of Dzyaloshinkii-Moriya interaction. Due to non-trivial topological properties, skyrmions manifest anomalous transport response to temperature gradients [9] and electric field [10–12]. Recently, Hamburg group demonstrated a controllable writing and deleting of single skyrmions on the surface of PdFe bilayer [13–15]. Skyrmions hold a great promise in applications such as spintronics, memory devices, et cetera [16, 17]. For example, interplay of a magnetic skyrmion and a topological insulator was recently considered in Ref. [18]. Coupling of magnetic films with skyrmions to novel materials may produce new functionalities in hybrid devices not available in the constituent materials taken separately.

In parallel, there has been a significant interest in superconductor-ferromagnet (SC-FM) heterostructures aimed at engineering topological superconductors [19, 20]. Discovery of the topological superconductivity would entail existence of the Majorana edge modes, which would pave the way to realizing topological quantum computing [21]. Motivated by the interest in skyrmions as well as SC-FM heterostructures we connect the two fields in the current work.

Below, we consider a FM film with a skyrmion proximity coupled to SC as shown in Fig. 1. We search for the states in SC localized around a skyrmion in a series of approximations. First, consider a limit of a small skyrmion, i.e. $R \ll \xi_{\rm sc}$. In this case, the approximation of the skyrmion field as a point magnetic moment is valid. Using this simplified model, we perform an analytical T-matrix calculation and find that skyrmion induces a bound state in the SC in a close analogy with the well-known Yu-Shiba-Rusinov states [22–25]. The SBS induces a resonance with a finite spectral width in a spin-polarized local density of states (SP LDOS). In contrast

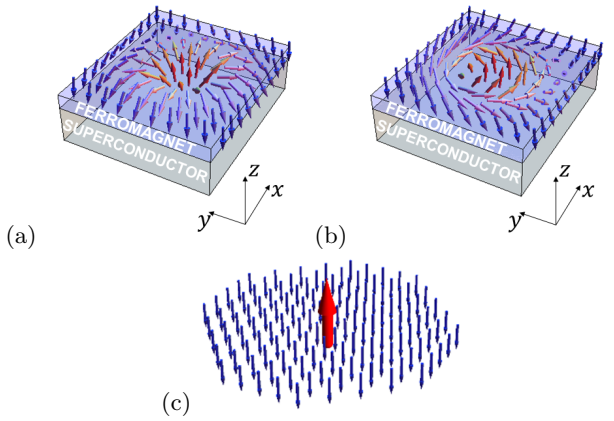

FIG. 1. (color online) (a,b) System under consideration: ferromagnetic (FM) film with a skyrmion proximity coupled to a superconductor (SC). (a) Néel-type skyrmion. (b) Bloch-type skyrmion. (c) Sketch of an approximation of a skyrmion as a local magnetic moment floating in a "ferromagnetic sea".

with the conventional YSR states, which are short-range, the SBS state is a long-range state with a power law decay. Therefore, in the presence of multiple skyrmions, the SC could mediate an effective long-range interaction between the skyrmions [26] when the SBS states overlap. Subsequently, we relax the requirement $R \ll \xi_{sc}$ and calculate the LDOS and wavefunctions for $R \sim \xi_{sc}$ numerically. We find that the SBS peak is populated by the multiple quasilocalized states corresponding to different angular momenta.

We also note that a few earlier papers have considered skyrmions in the context of superconductivity to some extent. Reference [27] studied the skyrmion-like solitons in the multiband superfluids and SCs. Paper [28] discussed a possibility of realizing a topological SC using a skyrmion lattice. The Josephson current through a magnetic skyrmion structure was considered in Ref. [29]. None of the papers up-to-date have addressed the conceptually simplest case of interaction between a single

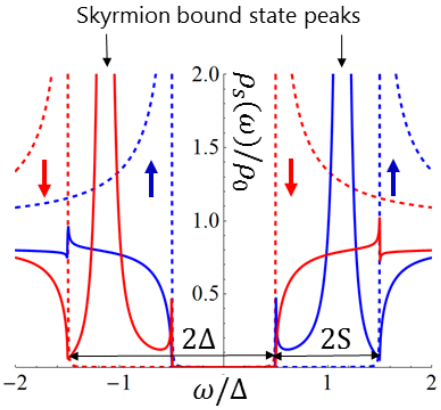

FIG. 2. (color online) Spin-polarized local density of states (SP LDOS) of SC away from the skyrmion (dashed) and at the skyrmion core (solid). The color of the curves encodes the spin polarization: blue for spin up and red for spin down as indicated by the arrows. The figure is obtained by using a model given by Eqs. (12) and (13) for the parameters $2S = \Delta = 0.1\mu$, $R = 2.5/p_F$, $S_0 = 5SR^2$, and $S_1 = 0.5SR^3$.

skyrmion and SC. This is the subject of the present paper.

Single skyrmion in a FM film.— Consider a FM film with the magnetization described by a three-dimensional vector $\boldsymbol{S}(\boldsymbol{r}) = (S_x, S_y, S_z)$ dependent on a two-dimensional (2D) spatial coordinate $\boldsymbol{r} = (x, y)$. The topological configurations of the field $\boldsymbol{S}(\boldsymbol{r})$ shown in Fig. 1(a) and (b) are referred to as skyrmions. Depending on a specific FM material, two distinct types of skyrmions are observed in experiment: the Néel (hedgehog) skyrmion and Bloch (spiral) skyrmion shown in Fig. 1(a) and (b), respectively. Although, the two types of skyrmions differ significantly in the orientation of the in-plane spins both are characterized by the same topological charge

$$Q = \frac{1}{4\pi}\int d^2r\, \hat{\boldsymbol{S}}\cdot(\nabla_x\hat{\boldsymbol{S}}\times\nabla_y\hat{\boldsymbol{S}}) = 1, \quad \hat{\boldsymbol{S}} = \frac{\boldsymbol{S}}{S}. \tag{1}$$

Thus, one can transform a Neel skyrmion into a Bloch skyrmion by a $\pi/2$ rotation [30] of the FM vector around the $\hat{\boldsymbol{z}}$ axis in the spin space without a change in the topological charge (1).

Superconductor proximity coupled to a ferromagnetic film.— Let us consider a heterostructure of a SC and FM with a skyrmion as shown in Fig. 1(a) and (b). The SC is described by the 4-by-4 Bogoliubov-de Gennes (BdG) Hamiltonian

$$H = \xi(\boldsymbol{p})\tau_z + \Delta\tau_x - \boldsymbol{S}(\boldsymbol{r})\cdot\boldsymbol{\sigma}, \tag{2}$$

$$\xi(\boldsymbol{p}) = \frac{\boldsymbol{p}^2}{2m} - \mu, \quad \boldsymbol{p} = -i(\nabla_x, \nabla_y). \tag{3}$$

Here, $\xi(\boldsymbol{p})$ describes the kinetic energy and Δ - the self-consistent superconducting gap, which we assume uniform in space; the term $\boldsymbol{S}(\boldsymbol{r})\cdot\boldsymbol{\sigma}$ describes the proximity coupling between the FM film and SC. We assume that the Zeeman splitting $S(\boldsymbol{r})$ does not exceed the Chandrasekhar-Clogston limit and $S < \Delta$. The Pauli matrices $\boldsymbol{\tau}$ and $\boldsymbol{\sigma}$ act, respectively, in the particle-hole and spin subspaces of the four-component spinor $\Psi = (\psi_\uparrow, \psi_\downarrow, \psi_\downarrow^\dagger, -\psi_\uparrow^\dagger)^T$. At this point, we do not include the effects of the spin-orbit coupling or spin-triplet superconductivity [30] in the model (2). We consider a case with a single Néel skyrmion centered at the origin, i.e. at $\boldsymbol{r} = 0$, and, so, assume the following profile of the FM vector

$$\boldsymbol{S}(\boldsymbol{r}) = S\left[\cos\phi(\boldsymbol{r})\sin\theta(\boldsymbol{r}),\, \sin\phi(\boldsymbol{r})\sin\theta(\boldsymbol{r}),\, \cos\theta(\boldsymbol{r})\right],$$
$$\phi(\boldsymbol{r}) = \arctan(y/x), \quad \theta(\boldsymbol{r}) = \pi\left[1 - \exp\left(-\frac{r^2}{R^2}\right)\right], \tag{4}$$

where R defines an effective radius of the skyrmion [31]. Let us compare the relevant spatial scales of the problem: the SC coherence length $\xi_{\rm sc} \approx v_F/\Delta$, the skyrmion radius R, and the Fermi length p_F^{-1}. Both the scales $\xi_{\rm sc}$ and R can vary from tens of nanometers to a micron depending on a specific material, whereas the Fermi length p_F^{-1} is typically smaller than the other two scales. In the regime $R \gg \xi_{\rm sc}$, the skyrmion can be viewed as a large FM domain pointing in the direction opposite to the rest of the system. Such a regime could be interesting in the context of topological SC [19]. For instance, it was recently shown [32–34] that a helical texture of spins in a one-dimensional (1D) chain of magnetic atoms on a surface of a SC generates an effective Rashba-like spin-orbit interaction responsible for the Majorana edge modes. Similar effective spin-orbit interaction is generated near a skyrmion and could give rise to non-trivial edge states localized at the edge of the skyrmion. We leave the discussion of this case for future works. In the current paper, we focus on the case of relatively small skyrmions, i.e. $R \lesssim \xi_{sc}$.

Multipole expansion of the skyrmion.— Let us now consider a case of a small skyrmion, i.e. $R \ll \xi_{\rm sc}$. In this limit, the superconductivity cannot "resolve" the fine details of the field $\boldsymbol{S}(\boldsymbol{r})$. We perform the multipole expansion of the skyrmion configuration (4) and approximate it as a point magnetic moment floating in a "ferromagnetic sea" as illustrated in Fig. 1(c)

$$\boldsymbol{S}_{\rm approx}(\boldsymbol{r}) = -S\hat{\boldsymbol{z}} + S_0\hat{\boldsymbol{z}}\delta^2(\boldsymbol{r}), \tag{5}$$

where S_0 is the zeroth moment of $\boldsymbol{S}(\boldsymbol{r})$

$$S_0 = \int d^2r\, \left[\boldsymbol{S}(\boldsymbol{r}) - \boldsymbol{S}(\infty)\right]_z \quad \sim \quad SR^2. \tag{6}$$

The formal domain of validity of the multipole expansion is $R \lesssim p_F^{-1} \ll \xi_{sc}$ [35]. The multipole expansion gives an elegant and physically transparent description of the system, and, for this reason, we use it even beyond the domain of validity. In the end of the paper, we present an exact numerical modeling and find a close agreement with a multipole analytical treatment.

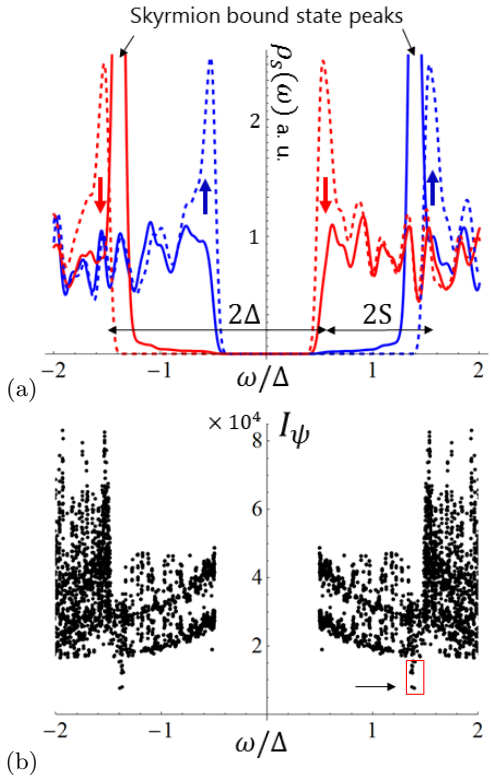

FIG. 3. (color online) Numerical modeling of a skyrmion. (a) Spin-polarized LDOS at the skyrmion core (solid) and away from the skyrmion (dashed). (b) The function I_ψ characterizing a degree of localization of each BdG wavefunctions ψ versus eigenenergy ω. Few of the quasilocalized wavefunctions emphasized by the red rectangle are shown in Fig. 4.

By performing the T-matrix calculation, we solve the model given by Eqs. (2) and (5), where we treat the local term $S_0\hat{\boldsymbol{z}}\delta^2(\boldsymbol{r})$ as a perturbation. We include the constant background magnetization $-S\hat{\boldsymbol{z}}$ in the BdG Hamiltonian $h(\boldsymbol{p}) = \xi(\boldsymbol{p})\tau_z + \Delta\tau_x + S\sigma_z$ and calculate an on-site matrix element of the bare Green's function $g(\omega,\boldsymbol{p}) = [\omega - h(\boldsymbol{p})]^{-1}$

$$g_0(\omega) = -\pi\rho_0 \sum_{\lambda=\pm1} \frac{1+\lambda\sigma_z}{2} \frac{\omega - \lambda S + \Delta\tau_x}{\sqrt{\Delta^2 - (\omega-\lambda S)^2}}, \qquad (7)$$

where $\rho = m/2\pi$ is the density of states. This Green's function describes a SC subject to a uniform background magnetization $-\hat{\boldsymbol{z}}S$ that shifts the spin subbands as shown with the dashed lines in Fig. 2. The density of states contains two interior and two exterior coherence peaks at the energies $\pm(\Delta - S)$ and $\pm(\Delta + S)$ correspondingly. Using Green's function (7) we calculate the T-matrix in the presence of a point magnetic moment $V(\boldsymbol{r}) = -S_0\,\sigma_z\delta^2(\boldsymbol{r})$ representing the skyrmion

$$T(\omega) = \frac{-S_0\sigma_z}{1 + S_0\sigma_z g_0(\omega)}. \qquad (8)$$

The poles of T-matrix give the energies of the skyrmion-induced bound states (SBS)

$$E^{\pm}_{\rm SBS} = \pm\left[S + \Delta\frac{1-(\pi\rho S_0)^2}{1+(\pi\rho S_0)^2}\right]. \qquad (9)$$

Let us trace the SBS energies as a function of increasing S_0, which is an implicit function of S and R according to Eq. (6). For small S_0, the SBS states lie at the outer coherence peaks at the energies $\pm(\Delta + S)$. With further increase of S_0, the SBS states split from the outer coherence peak and move to the inner coherence peaks [36]. The spin-polarization of the SBS states is determined by the spin-polarization of the bulk bands that they split from: the positive (negative) SBS state is "up" ("down") spin-polarized. The SBS states resemble closely the well-known Yu-Shiba-Rusinov (YSR) states [22–25] localized around magnetic impurities in SC. The main difference is that the YSR energies reside inside the actual spectral gap, whereas the SBS energies lie in the window of energies $\Delta + S > |E^{\pm}_{\rm SBS}| > \Delta - S$, which is also filled with a continuum of delocalized states of the opposite spin polarization.

Now let us show that SBS gives a resonance of finite spectral width due to the coupling with the continuum of delocalized states. Indeed, the skyrmion has in-plane spins at $r \approx R$ that couple the spin-up and spin-down sectors of the Hamiltonian. In order to capture this effect we append the multipole expansion (5) with a next order term representing the radial in-plane spins of the skyrmion.

$$\boldsymbol{S}_{\rm approx}(\boldsymbol{r}) = -S\hat{\boldsymbol{z}} + S_0\hat{\boldsymbol{z}}\delta^2(\boldsymbol{r}) - S_1\boldsymbol{\nabla}\delta^2(\boldsymbol{r}), \qquad (10)$$

where $\boldsymbol{\nabla} = (\nabla_x, \nabla_y)$ and S_1 is the first moment of the original skyrmion configuration $\boldsymbol{S}(\boldsymbol{r})$

$$S_1 = \frac{1}{2}\int d^2r\,[\boldsymbol{S}(\boldsymbol{r}) - \boldsymbol{S}(\infty)]\cdot\boldsymbol{r} \quad \sim \quad SR^3. \qquad (11)$$

In the Supplemental Material, we solve the Lippmann-Schwinger equation for the T-matrix in the presence of the perturbation $V(\boldsymbol{r}) = -S_0\,\sigma_z\delta^2(\boldsymbol{r}) + S_1(\boldsymbol{\sigma}\cdot\boldsymbol{\nabla})\delta^2(\boldsymbol{r})$, which yields

$$T(\omega) = \frac{-S_0\sigma_z + S_1^2 p_F^2 \bar{g}_0(\omega)}{1 + S_0\sigma_z g_0(\omega) - S_1^2 p_F^2\,\bar{g}_0(\omega)\,g_0(\omega)}. \qquad (12)$$

Here, the Green's function $\bar{g}_0(\omega) = \frac{1}{2}\sum_{j=x,y}\sigma_j g_0(\omega)\sigma_j$ describes the bands with opposite spin polarization $\sigma_z \to -\sigma_z$. Using Eq. (12) we calculate SP LDOS

$$\rho_s(\omega) = \qquad (13)$$
$$-\frac{1}{\pi}\,{\rm Im\,Tr}\left\{\frac{1+\tau_z}{2}\,\frac{1+\sigma_s}{2}\,[g_0(\omega) + g_0(\omega)T(\omega)g_0(\omega)]\right\},$$

where $s = x, y, z$ denotes the spin projection axis. We plot LDOS (13) with solid lines in Fig. 2 and compare it with LDOS away from the skyrmion shown with dashed lines. We observe that the peaks corresponding to the

SBS resonances have finite spectral width. Indeed, the denominator of T-matrix (12) has an extra term compared to that of Eq. (8). The first two terms in the denominator of (12) give the SBS energies (9), whereas the last term $S_1^2 p_F^2\, \bar{g}_0(\omega)\, g_0(\omega)$ is imaginary and defines the spectral width of the SBS resonance observed in Fig. 2.

Numerical analysis.— So far we have analyzed the skyrmion using the analytical multipole approximation. Now let us present the results of an exact numerical modeling. We set the BdG Hamiltonian on the N-by-N tight-binding square lattice with parameters: the lateral size N = 200, nearest neighbor coupling t, on-site superconducting pairing and Zeeman coupling $\Delta = 2S = 0.1t$, and chemical potential $\mu = -3t$. This choice of parameters corresponds to $\xi_{\rm sc} \approx 17a$ in the units of the elementary cell constant a. The skyrmion is described by the vector $\boldsymbol{S}(\boldsymbol{r})$ given by Eq. (4) with the effective radius $R = 6a$, so that $2R \sim \xi_{\rm sc}$. From the numerical wavefunctions, we calculate SP LDOS, apply the Gaussian smoothing kernel and plot the resulting SP LDOS in Fig. 3(a). We use the same plotting style as in Fig. 2: solid (dashed) line represents LDOS at (away from) the skyrmion, whereas colors encode spin polarizations. We observe that the calculated LDOS is consistent with the results of the analytical calculation. Away from the skyrmion, SP LDOS contains the shifted spin subbands. At the skyrmion core, the skyrmion induces a strong resonance in the energy window $\Delta - S < |\omega| < \Delta + S$. In order to further analyze the numerical wavefunctions $\psi(\boldsymbol{r})$, we also calculate the following expression

$$I_\psi = \frac{1}{\sum_{\boldsymbol{r}} |\psi(\boldsymbol{r})|^4}, \tag{14}$$

where the sum is carried over all lattice sites $\boldsymbol{r}$. The function I_ψ characterizes a degree of a localization of the wavefunction $\psi(\boldsymbol{r})$ [37]. The function is small $I_\psi \sim 1$ for an extremely localized wavefunction and large $I_\psi \sim N^2$ for a delocalized wavefunction. For each numerical BdG wavefunction $\psi(\boldsymbol{r})$, we plot I_ψ against the eigenenergy in Fig. 3(b) and superpose it with SP LDOS shown in panel (a). We observe a number of distinct quasilocalized states that stand out from the rest of states as emphasized by the red rectangle in Fig. 3(b). These states have the energy of the SBS peak, and their number grows with a skyrmion size. We visualize the spatial profile of the electron part of the BdG wavefunction $|\Psi(\boldsymbol{r})|^2 = |u_\uparrow(\boldsymbol{r})|^2 + |u_\downarrow(\boldsymbol{r})|^2$ for a few of these states in Fig. 4. In contrast with the analytical results, we find a wavefunction with multiple lobes corresponding to a higher angular momentum state, shown in panel (a), as well as a state with a single peak, shown in panel (d). It is known that higher angular momentum states do form bound states. Analytic solution presented above is based on the on-site T matrix and is not sufficient to capture the higher-angular-momentum bound states.

We also observe that all wavefunctions in Fig. 4 exhibit characteristic oscillations at the scale $\xi_{\rm sc}$. In order to understand this behavior, consider a

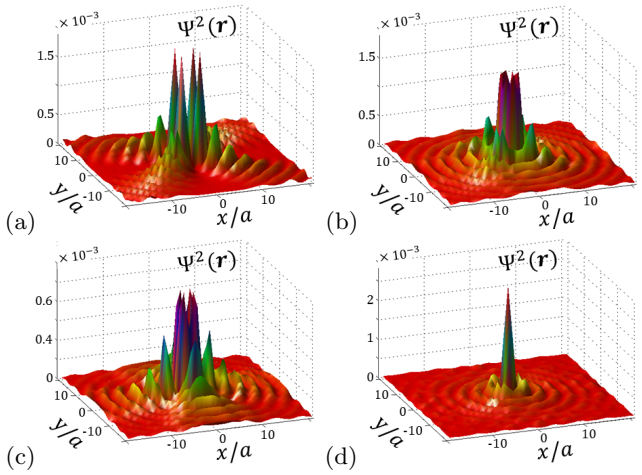

FIG. 4. (Color online) Spatial profile of the quasilocalized wavefunctions obtained numerically, which are indicated in Fig. 3(b). The wavefunctions are shown in the order of increasing I_ψ.

generic wavefunction of an impurity induced state $\Psi_\lambda(\boldsymbol{r}) \sim e^{ip_F r - r\sqrt{\Delta^2 - (\omega - \lambda S)^2}/v_F}/\sqrt{r}$, where λ denotes the eigenvalues of σ_z operator. The terms in the exponent term describe behavior at two scales p_F^{-1} as well as $\xi_{\rm sc}$. For clarity, let us focus on the positive SBS state, i.e. $\omega = E^+_{\rm SBS}$. From the point of view of spin-up subband, i.e. $\lambda = 1$, the SBS is a subgap state, i.e. $|\omega - S| < \Delta$, and so the square root term in $\Psi_+(\boldsymbol{r})$ gives an exponentially localized wavefunction. However from the point of view of spin-down subband, i.e. $\lambda = -1$, the SBS is a supragap state, i.e. $\omega + S > \Delta$, and, so, the square root in $\Psi_-(\boldsymbol{r})$ gives oscillations at the scale of ξ_{sc} superimposed with a long-range $1/\sqrt{r}$ decay. These oscillations as well the long-range behavior can be seen in Fig. 4.

Recently, a new YSR mechanism of interaction between magnetic impurities mediated by a superconductor was proposed [26]. If the impurities a close enough, the wavefunctions of the corresponding YSR states overlap. The hybridization between the YSR states has an energetic cost and defines an effective interaction between impurities that could even be stronger than the conventional RKKY interaction. Similar reasoning could be used for the case of multiple skyrmions. In this case, an overlap of the power-law SBS wavefunctions will result in an effective long-range interaction between distinct skyrmions. We estimate a magnitude of this interaction in the Supplemental Material.

Conclusion and Outlook.— In this paper, we predict the new skyrmion bound state (SBS) in SC proximity coupled to the FM film with a skyrmion texture. We calculate SP LDOS and show the signatures of SBS in the tunneling spectrum that could be measured by the spin-polarized scanning tunneling microscopy (SP STM). The skyrmion induces a resonance in between the spin-split coherence peaks corresponding to the opposite spin polarizations. We show that the wavefunction of SBS

is quasilocalized, i.e., decays as $1/\sqrt{r}$. Thus in the case of the two skyrmions, their SBS wavefunctions will overlap and induce a long-range interaction between the skyrmions [26, 38]. The details of the long-range interaction will be explored in a subsequent publication.

We hope that the current paper will be a first step in studying SC-skyrmion heterostructures and there is a number intriguing questions to explore. For instance, SC could induce an effective Dzyaloshinkii-Moriya interaction between ferromagnetic spin especially in non-centrosymmetric materials and, thus, stabilize the skyrmion phase. It would also be interesting to consider the connection with the topological SC hybrid systems [19, 28].

After this manuscript was submitted, we learned of further theoretical studies [39, 40] of the hybrid skyrmion-SC heterostructures. Authors of Ref. [39] found the Majorana bound state solution in the vicinity of the skyrmions of higher winding numbers. Authors of Ref. [40] studied an interaction between a skyrmion and vortex in a type-II superconductor.

We thank R. Wiesendanger, S. Fujimoto, J. Wiebe, J. Zang, A. Saxena, H. Hurst, Y. Tserkovnyak, S. Lin and L. Bulaevskii for valuable discussions and comments. This work was supported by US DOE BES E304 (S.S.P. and A.V.B.) and by the Grant-in-Aid for Research Activity Start-up (No. 15H06858) (S.N.).

[1] T. H. Skyrme, "A non-linear field theory," Proc. R. Soc. Lond. Ser. A **260**, 127 (1961).
[2] A. N. Bogdanov and D. A. Yablonskii, "Thermodynamically stable "vortices" in magnetically ordered crystals. The mixed state of magnets." Sov. Phys. JETP **68**, 101 (1989).
[3] U. K. Rössler, A. N. Bogdanov, and C. Pfleiderer, "Spontaneous skyrmion ground states in magnetic metals." Nature **442**, 797 (2006).
[4] S. Mühlbauer, B. Binz, F. Jonietz, C. Pfleiderer, A. Rosch, A. Neubauer, R. Georgii, and P. Böni, "Skyrmion lattice in a chiral magnet." Science **323**, 915 (2009).
[5] W. Münzer, A. Neubauer, T. Adams, S. Mühlbauer, C. Franz, F. Jonietz, R. Georgii, P. Böni, B. Pedersen, M. Schmidt, A. Rosch, and C. Pfleiderer, "Skyrmion lattice in the doped semiconductor $Fe_{1-x}Co_xSi$," Phys. Rev. B **81**, 041203 (2010).
[6] X. Z. Yu, N. Kanazawa, Y. Onose, K. Kimoto, W. Z. Zhang, S. Ishiwata, Y. Matsui, and Y. Tokura, "Near room-temperature formation of a skyrmion crystal in thin-films of the helimagnet FeGe," Nat. Mater. **10**, 106 (2011).
[7] S. Heinze, K. von Bergmann, M. Menzel, J. Brede, A. Kubetzka, R. Wiesendanger, G. Bihlmayer, and S. Blugel, "Spontaneous atomic-scale magnetic skyrmion lattice in two dimensions," Nat. Phys. **7**, 713–718 (2011).
[8] S. Seki, X. Z. Yu, S. Ishiwata, and Y. Tokura, "Observation of Skyrmions in a Multiferroic Material," Science **336**, 198 (2012).
[9] F. Jonietz, S. Mhlbauer, C. Pfleiderer, A. Neubauer, W. Mnzer, A. Bauer, T. Adams, R. Georgii, P. Bni, R. A. Duine, K. Everschor, M. Garst, and A. Rosch, "Spin Transfer Torques in MnSi at Ultralow Current Densities," Science **330**, 1648 (2010).
[10] A. Neubauer, C. Pfleiderer, B. Binz, A. Rosch, R. Ritz, P. G. Niklowitz, and P. Böni, "Topological Hall Effect in the A Phase of MnSi," Phys. Rev. Lett. **102**, 186602 (2009).
[11] J. Zang, M. Mostovoy, J. H. Han, and N. Nagaosa, "Dynamics of skyrmion crystals in metallic thin films," Phys. Rev. Lett. **107**, 136804 (2011).
[12] S.-Z. Lin, C. Reichhardt, C. D. Batista, and A. Saxena, "Particle model for skyrmions in metallic chiral magnets: Dynamics, pinning, and creep," Phys. Rev. B **87**, 214419 (2013).
[13] N. Romming, C. Hanneken, M. Menzel, J. E. Bickel, B. Wolter, K. von Bergmann, A. Kubetzka, and R. Wiesendanger, "Writing and Deleting Single Magnetic Skyrmions," Science **341**, 636 (2013).
[14] K. von Bergmann, A. Kubetzka, O. Pietzsch, and R. Wiesendanger, "Interface-induced chiral domain walls, spin spirals and skyrmions revealed by spin-polarized scanning tunneling microscopy," J. Phys.: Condens. Matter **26**, 394002 (2014).
[15] N. Romming, A. Kubetzka, C. Hanneken, K. von Bergmann, and R. Wiesendanger, "Field-Dependent Size and Shape of Single Magnetic Skyrmions," Phys. Rev. Lett. **114**, 177203 (2015).
[16] A. Fert, V. Cros, and J. Sampaio, "Skyrmions on the track," Nat. Nano **8**, 152–156 (2013).
[17] N. Nagaosa and Y. Tokura, "Topological properties and dynamics of magnetic skyrmions," Nat. Nanotechnol. **8**, 899 (2013).
[18] H. M. Hurst, D. K. Efimkin, J. Zang, and V. Galitski, "Charged skyrmions on the surface of a topological insulator," Phys. Rev. B **91**, 060401 (2015).
[19] J. Alicea, "New directions in the pursuit of Majorana fermions in solid state systems." Rep. Prog. Phys. **75**, 076501 (2012).
[20] C. W. J. Beenakker, "Random-matrix theory of Majorana fermions and topological superconductors," Rev. Mod. Phys. **87**, 1037 (2015).
[21] C. Nayak, S. H. Simon, A. Stern, M. Freedman, and S. Das Sarma, "Non-abelian anyons and topological quantum computation," Rev. Mod. Phys. **80**, 1083–1159 (2008).
[22] L. Yu, "Bound state in superconductors with paramagnetic impurities," Acta Phys. Sin. **21**, 75 (1965).
[23] H. Shiba, "Classical Spins in Superconductors," Prog. Theor. Phys. **40**, 435 (1968).
[24] A. I. Rusinov, "Superconductivity near a paramagnetic impurity," JETP Lett. **9**, 85 (1969).
[25] A. V. Balatsky, I. Vekhter, and J.-X. Zhu, "Impurity-induced states in conventional and unconventional superconductors," Rev. Mod. Phys. **78**, 373 (2006).
[26] N. Y. Yao, L. I. Glazman, E. A. Demler, M. D. Lukin, and J. D. Sau, "Enhanced Antiferromagnetic Ex-

change between Magnetic Impurities in a Superconducting Host," Phys. Rev. Lett. **113**, 087202 (2014).
[27] J. Garaud, J. Carlström, and E. Babaev, "Topological solitons in three-band superconductors with broken time reversal symmetry," Phys. Rev. Lett. **107**, 197001 (2011).
[28] S. Nakosai, Y. Tanaka, and N. Nagaosa, "Two-dimensional p-wave superconducting states with magnetic moments on a conventional s-wave superconductor," Phys. Rev. B **88**, 180503 (2013).
[29] T. Yokoyama and J. Linder, "Josephson effect through magnetic skyrmions," Phys. Rev. B **92**, 060503 (2015).
[30] Note that for the case of a spin-singlet SC given by Eq. (2), the Bloch and the Neel skyrmions are equivalent since they can be related by a continuous $\pi/2$-rotation around the z-axis in the spin space $U = \exp(-i\pi\sigma_z/4)$. In the presence of either the spin-triplet pairing or the spin-orbit interaction, the effects of the two types of skyrmions are different.
[31] We expect that a different spatial dependency of the azimuthal angle (4) will not change the results significantly.
[32] B. Braunecker and P. Simon, "Interplay between classical magnetic moments and superconductivity in quantum one-dimensional conductors: Toward a self-sustained topological majorana phase," Phys. Rev. Lett. **111**, 147202 (2013).
[33] J. Klinovaja, P. Stano, A. Yazdani, and D. Loss, "Topological Superconductivity and Majorana Fermions in RKKY Systems," Phys. Rev. Lett. **111**, 186805 (2013).
[34] M. M. Vazifeh and M. Franz, "Self-organized topological state with majorana fermions," Phys. Rev. Lett. **111**, 206802 (2013).
[35] The domain of applicability can also be extended to $p_F^{-1} < R \ll \xi_{sc}$ with some modification of the theory.
[36] Although Eq. (9) suggests that the SBS states may go inside the actual gap for large enough S_0, i.e. $|E^{\pm}_{\rm SBS}| < \Delta - S$, the multipole approximation of a skyrmion (5) is no-longer valid in this regime and, thus, does not give a reliable estimate of the SBS energy. In practice, by performing a numerical modeling, we never observe the SBS peaks inside the actual spectral gap, i.e. in the window of energies $|E^{\pm}_{\rm SBS}| < \Delta - S$.
[37] The function I_ψ^{-1} is commonly referred to as the inverse participation ratio in the literature on localization phenomena.
[38] G. C. Ménard, S. Guissart, C. Brun, S. Pons, V. S. Stolyarov, F. Debontridder, M. V. Leclerc, E. Janod, L. Cario, D. Roditchev, P. Simon, and T. Cren, "Coherent long-range magnetic bound states in a superconductor," Nat. Phys. **advance online publication** (2015), letter.
[39] G. Yang, P. Stano, J. Klinovaja, and D. Loss, "Majorana bound states in magnetic skyrmions," arXiv:1602.00968.
[40] K. M. D. Hals, M. Schecter, and M. S. Rudner, "Composite topological excitations in ferromagnet-superconductor heterostructures," arXiv:1603.07550.
[41] A. V. Shytov, D. A. Abanin, and L. S. Levitov, "Long-range interaction between adatoms in graphene," Phys. Rev. Lett. **103**, 016806 (2009).
[42] D. A. Abanin and D. A. Pesin, "Ordering of magnetic impurities and tunable electronic properties of topological insulators," Phys. Rev. Lett. **106**, 136802 (2011).

Appendix A: T-matrix derivation

In this section, we provide details on the derivation of the T-matrix (12) for the model given by Eqs. (2) and (10). In the momentum space, the local terms defined via the delta functions in Eq. (10) generate the following perturbation

$$V(\boldsymbol{p}) = -S_0\,\sigma_z + i\,S_1\,\boldsymbol{\sigma}\cdot\boldsymbol{p}. \tag{A1}$$

Using Eq. (A1) and the bare Green's function (7), we write the Lippmann-Schwinger integral equation for the T-matrix

$$T\left(\boldsymbol{p}^{\rm out},\boldsymbol{p}^{\rm in}\right) = V\left(\boldsymbol{p}^{\rm out}-\boldsymbol{p}^{\rm in}\right) + \int \frac{d^2p'}{(2\pi)^2}\,V\left(\boldsymbol{p}^{\rm out}-\boldsymbol{p}'\right)g(\omega,\boldsymbol{p}')T\left(\boldsymbol{p}',\boldsymbol{p}^{\rm in}\right). \tag{A2}$$

Since in the case of the superconductivity we are interested in the scatterings close to the Fermi surface, we use $\boldsymbol{p}^{\rm out} = p_F\,\boldsymbol{n}^{\rm out}$ and $\boldsymbol{p}^{\rm in} = p_F\,\boldsymbol{n}^{\rm in}$, where the in-plane unit vectors $\boldsymbol{n}^{\rm out}$ and $\boldsymbol{n}^{\rm in}$ determine the direction of scattering on the Fermi surface. Then, we seek the T-matrix in the following form

$$T\left(\boldsymbol{n}^{\rm out},\boldsymbol{n}^{\rm in}\right) = T^0 + T^1_i n^{\rm out}_i + T^{1\,\dagger}_j n^{\rm in}_j + T^2_{ij}\,n^{\rm out}_i n^{\rm in}_j, \tag{A3}$$

where T, T^1_i, T^2_{ij} are the 4-by-4 matrices in the $\sigma\otimes\tau$ space, which give the expansion of the T-matrix in vectors $n^{\rm out}_i$ and $n^{\rm in}_j$. We substitute the ansatz (A3) in Eq. (A2) and rewrite the integral equation as

$$T\left(\boldsymbol{n}^{\rm out},\boldsymbol{n}^{\rm in}\right) = -S_0\,\sigma_z + i\,S_1 p_F\,\sigma_i\left(n^{\rm out}_i - n^{\rm in}_i\right) \tag{A4}$$

$$+\int d\boldsymbol{n}'\left[-S_0\,\sigma_z + i\,S_1 p_F\,\sigma_i\left(n^{\rm out}_i - n'_i\right)\right]g_0(\omega)\left[T^0 + T^1_j n'_j + T^{1\,\dagger}_j n^{\rm in}_j + T^2_{kj}\,n'_k n^{\rm in}_j\right], \tag{A5}$$

where after an integration in the radial direction p' the Green's function in the momentum space $g(\omega,\boldsymbol{p}')$ transforms into an on-site matrix of the Green's functions $g_0(\omega)$. Next, we take an integral over the angular variable $\boldsymbol{n}'$, i.e.

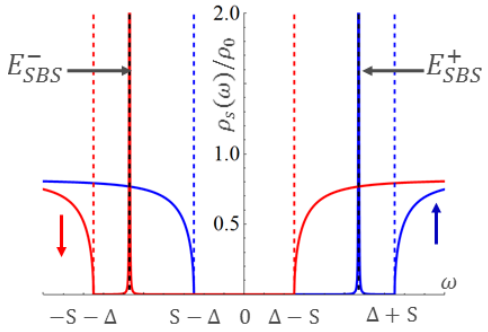

FIG. 5. (color online) Spin-polarized local density of states in the absence of the in-plane spins, i.e. at $S_1 = 0$. The localized skyrmion bound states (SBS) do not couple to the delocalized states of the opposite spin-polarization and are described by the sharp poles given by Eq. (B3). Blue and red colors encode the up and down spin polarizaion.

$\int d\boldsymbol{n}'\, n'_i = 0$ and $\int d\boldsymbol{n}'\, n'_i n'_j = \delta_{ij}/2$, and obtain a closed set of equations for the unknown matrices

$$T^0 = -S_0\sigma_z - S_0\sigma_z g_0\, T^0 - \frac{1}{2} i S_1 p_F\, \sigma_i g_0\, T^1_i, \tag{A6}$$

$$T^1_i = i S_1 p_F\, \sigma_i \left[1 + g_0(\omega)\, T^0\right], \tag{A7}$$

$$T^2_{ij} = i S_1 p_F\, \sigma_i g_0(\omega)\, T^{1\,\dagger}_j. \tag{A8}$$

Solution of the Eqs. (A6)-(A8) gives

$$T^0 = \left[-S_0\sigma_z + S_1^2 p_F^2 \bar{g}_0(\omega)\right] D, \qquad T^1_i = i S_0 p_F\, \sigma_i\, D, \qquad T^2_{ij} = S_1^2 p_F^2\, \sigma_i g_0 D \sigma_j, \tag{A9}$$
$$\text{where } D = \left[1 + S_0\sigma_z g_0 - S_1^2 p_F^2\, \bar{g}_0(\omega)\, g_0(\omega)\right]^{-1}.$$

Note that the relative order of the matrices in Eq. (A9) is important because the spin Pauli matrices do not commute. For brevity, $\bar{g}_0(\omega) = \frac{1}{2}\sum_{j=x,y} \sigma_j g_0(\omega)\sigma_j$ denotes the Green's function obtained from g_0 by replacing $\sigma_z \to -\sigma_z$. So, in the presence of the skyrmion, the Green's function becomes

$$G(\omega, \boldsymbol{p}^1, \boldsymbol{p}^2) = g(\omega, \boldsymbol{p}^1)\,(2\pi)^2 \delta(\boldsymbol{p}^1 - \boldsymbol{p}^2) + g(\omega, \boldsymbol{p}^1) T(\boldsymbol{p}^1, \boldsymbol{p}^2) g(\omega, \boldsymbol{p}^2), \tag{A10}$$

using which the spin-polarized local density of states (SP-LDOS) can be expressed

$$\rho_s(\omega, \boldsymbol{r}) = -\frac{1}{\pi}\,\mathrm{Im} \lim_{\omega\to\omega+i\delta} \mathrm{Tr}\left[\frac{1+\tau_z}{2}\,\frac{1+\sigma_s}{2}\int \frac{d^2p^1\, d^2p^2}{(2\pi)^4} e^{i(\boldsymbol{p}^1 - \boldsymbol{p}^2)\boldsymbol{r}} G(\omega, \boldsymbol{p}^1, \boldsymbol{p}^2)\right] \tag{A11}$$

where $s = x, y, z$ denotes the spin quantization axis. At the skyrmion core, i.e. at $\boldsymbol{r} = 0$, only the T^0 part of the T-matrix contributes to local density of states

$$\rho_s(\omega, 0) = -\frac{1}{\pi}\,\mathrm{Im} \lim_{\omega\to\omega+i\delta} \mathrm{Tr}\left\{\frac{1+\tau_z}{2}\,\frac{1+\sigma_s}{2}\left[g_0(\omega) + g_0(\omega)\frac{-S_0\sigma_z + S_1^2 p_F^2 \bar{g}_0(\omega)}{1 + S_0\sigma_z g_0(\omega) - S_1^2 p_F^2\, \bar{g}_0(\omega)\, g_0(\omega)} g_0(\omega)\right]\right\} \tag{A12}$$

whereas T^1 and T^2 drop out. Equation (A12) gives the expression in Eq. (12).

Appendix B: Interaction between skyrmions

In this section, we address the question of interaction between skyrmions mediated by a superconductor. Let us list a few recent works relevant for the discussion below. It was generally believed that the YSR states are localized on an atomic scale [25]. However, it was demonstrated recently that, in the case of a quasi-2D superconductor, the YSR states are rather extended and survive at a scale of superconducting coherence length [38]. This demonstrates for the first time the extended nature of the YSR states and hints that the long-range power-law SBS wavefunctions, predicted in the current work, could, in principle, be measured using STM. Authors of Ref. [26] suggested a new mechanism by

which a superconducting host could mediate an effective interaction between embedded impurities whenever the YSR states associated with the distinct impurities overlap. They argued that the YSR interaction could even dominate the conventional RKKY interaction, where the YSR states are sufficiently close to the center of superconducting gap. To sum up, we base our claim of interaction between the skyrmion on these to works [26, 38]. First, the YSR states are extended object as was demonstrated in Ref. [38]. Second, superconductivity mediates an effective interaction between magnetic impurities, when the corresponding YSR wavefunctions overlap. Analogously, since the SBS states have long-range power-law decay, the superconductivity should mediate a long-range interaction.

In order to estimate the superconductivity-induced interaction between skyrmions we use the formalism of TGTG formula frequently discussed in the context of Casimir interaction. It was also used to describe the interaction mediated by electrons between impurities in graphene [41] and topological insulators [42]. At zero temperature $T = 0$, the free energy interaction between the skyrmions can be conveniently expressed as

$$U_{\rm int}(r) = \frac{1}{\pi}\int_{-\infty}^{0} d\omega \ {\rm Im\,Tr\,Log}\ \left[1 - g_{\boldsymbol{r}}(\omega)T_1(\omega)g_{-\boldsymbol{r}}(\omega)T_2(\omega)\right], \tag{B1}$$

where integral is taken over all negative energies, i.e. filled states, in the Bogolyubov-de Gennes formulation. The derivation of formula B1 as well as equivalence to the approach of Ref. [26] are shown in Sec. C. In Eq. (B1), T_1 and T_2 are the T-matrices corresponding to individual skyrmions, and the Green's function $g_{\boldsymbol{r}}$ is calculated in the real space for large $r \gtrsim \xi_{\rm sc} \gg p_F^{-1}$

$$g_{\boldsymbol{r}}(\omega) = -\sqrt{\frac{2\pi}{p_F r}}\sum_{\lambda=\pm1}\frac{1+\lambda\sigma_z}{2}\left[\tau_z\cos\left(p_F r+\frac{\pi}{4}\right) + \frac{\omega-\lambda S+\Delta\tau_x}{\sqrt{\Delta^2-(\omega-\lambda S)^2}}\sin\left(p_F r+\frac{\pi}{4}\right)\right]\rho_0\, e^{-r\sqrt{\Delta^2-(\omega-\lambda S)^2}/v_F}. \tag{B2}$$

Here, the projector $\frac{1+\lambda\sigma_z}{2}$ selects the spin-up and down sectors of the Hamiltonian, which are shifted in energy due to the constant FM field $-S\,\hat{\boldsymbol{z}}$ as discussed in the paper. Note a square root term in the exponent of Eq. (B2). For $|\omega-\lambda S| < \Delta$, the exponent produces an exponential decay at the scale of $r \sim v_F/\sqrt{\Delta^2-(\omega-\lambda S)^2}$. In contrast, the square root becomes purely imaginary $-i\,{\rm sgn}(\omega-\lambda S)\sqrt{(\omega-\lambda S)^2-\Delta^2}$ for $|\omega-\lambda S| > \Delta$, and so the exponential term gives periodic oscillations rather than exponential decay. This observation motivates the explanation of the long-range coupling: the SBS states couple to the delocalized states of the opposite spin polarization, for which the square root is imaginary. Then the Green's function, which has a long-range power-law behavior, can propagate between the skyrmions at large distances $r > \xi$ and, thus, couple their SBS states and generate an effective interaction between skyrmions.

The T-matrix given in Eq. (A9) has a quite involved form. For simplicity, let us demonstrate the long-range interaction between skyrmions perturbatively in S_1. First, at $S_1 = 0$, i.e. where the in-plane scattering is neglected, the T-matrix (A9) reduces to a simpler Eq. (8) of the main text. The corresponding SP LDOS is shown in Fig. (5). The SBS states are represented by sharp peaks in the density of states which lie in the energy windows between the Zeeman split coherence peaks, i.e. $\Delta + S > |E^{\pm}_{\rm SBS}| > \Delta - S$. In this approximation, the scattering by the in-plane spins is absent, and, therefore, the SBS states do not couple to the delocalized states of the opposite spin-polarization. Now, we consider the higher-order order terms of the T-matrix expansion in S_1. We look for the terms that would couple the SBS states to the delocalized states of the opposite spin polarization. In the second-order in S_1, there is one such term generated by the contribution T^2_{ij} in Eq. (A9). So, in the vicinity of the energy close to the SBS states, the relevant part of the T-matrix can be written as

$$T(\boldsymbol{n}^{\rm out},\boldsymbol{n}^{\rm in}) \to \sigma_i n_i^{\rm out}\left[S_1^2\sum_{\lambda=\pm1}\frac{1+\lambda\tau_x}{2}\frac{1+\lambda\sigma_z}{2}\ \frac{\alpha}{\omega-E^{\lambda}_{\rm SBS}}\right]\sigma_j n_j^{\rm in} \tag{B3}$$

where the terms $\frac{1+\lambda\tau_x}{2}$ and $\frac{1+\lambda\sigma_z}{2}$ are the projectors in the Nambu and spin space, whereas constant α gives a strength of the SBS poles. Observe that Eq. (B3) is dressed with the in-plane Pauli matrices σ_i on both sides of the expression. The in-plane Pauli matrices $\sigma_i = (\sigma_x, \sigma_y)$ flip the spin σ_z and, thus, couple the SBS poles to the background delocalized states. Then, we substitute Eqs. (B2) and (B3) in Eq. (B1). The integral in Eq. (B1) is dominated by the poles in the T-matrix, so we approximate the integrand

$${\rm Im\,Tr\,Log}\left[1 - \beta\frac{S_1^4}{p_F r}\sum_{\lambda=\pm1}\frac{1+\lambda\sigma_z}{2}\frac{1}{\left(\omega-E^{-\lambda}_{\rm SBS}\right)^2}e^{-i\lambda r\sqrt{\left(E^{-\lambda}_{\rm SBS}-\lambda S\right)^2-\Delta^2}/v_F}\right], \tag{B4}$$

where β is a constant absorbing other parameters. Observe, that the argument in the exponent is imaginary. Since the integral in Eq. (B1) runs over negative energies, $\lambda = 1$ dominates the integral and we focus only at the vicinity of ω around $E^-_{\rm SBS}$. So, after shifting the integration variable $\omega - E^-_{\rm SBS} \to \omega$, and reexpressing the imaginary part of the logarithm, we rewrite the integral as

$$U_{\rm int}(r) = \frac{1}{\pi}\int_{-\infty}^{\infty} d\omega \,\mathrm{atan}\left[\frac{\sin\kappa r}{\frac{p_F r}{\beta S_1^4}\omega^2 - \cos\kappa r}\right] = S_1^2\sqrt{\frac{\beta}{p_F r}} I(\kappa r),, \tag{B5}$$

where $\kappa = \sqrt{\left(E^-_{\rm SBS} - S\right)^2 - \Delta^2}/v_F$, and $I(r) = \frac{1}{\pi}\int_{-\infty}^{\infty} dx\,\mathrm{atan}\left[\frac{\sin\kappa r}{x^2-\cos\kappa r}\right]$ is a periodic function of κr: $I(\kappa r) = 2\cos\left(\frac{\kappa r}{2}\right)$ for $4\pi n{+}2\pi > \kappa r > 4\pi n$, and $I(\kappa r) = -2\cos\left(\frac{\kappa r}{2}\right)$ for $4\pi n{+}4\pi > \kappa r > 4\pi n{+}2\pi$. So, we find that interaction between skyrmions (B5) decays as $1/\sqrt{r}$ and oscillates at a scale of $1/\kappa$. In colloquial terms, the oscillating long-range SBS wavefunctions corresponding to distinct skyrmions determine the effective interaction between skyrmions. Note that, we have calculated the contribution to the energy only due to the subgap states, and neglected the supragap states. The full analysis using Eqs. (A9) and (B1) will be given in a subsequent work.

Appendix C: Derivation of the TGTG formula (B1).

The TGTG formula (B1) has been used extensively for calculation of Casimir forces. Authors [41, 42] also used it to calculate the electron-mediated interaction between impurities in graphene and topological insulators. For completeness, we give a derivation of the TGTG formula in the context of superconductivity.

Impurities (or any other local perturbation) brought in a superconductor modify the density of states $\delta\rho(\omega)$ and cause an overall energy shift [26]

$$U = \int_{-\infty}^{0} d\omega\,\omega\,\delta\rho(\omega). \tag{C1}$$

The density of states can be reexpressed using the bare Green's function g and T-matrix T

$$\delta\rho = -\frac{1}{\pi}\mathrm{Im\,Tr}\,[gTg] = -\frac{1}{\pi}\mathrm{Im\,Tr}\,\left[g\,V\,(1-gV)^{-1}\,g\right], \tag{C2}$$

where V describes the effect of two (or arbitrary number of) impurities. Using the cyclic permutations within trace, we bring the two Green's functions together, use an identity $\frac{\partial g}{\partial\omega} = -g^2$ and finally obtain as follows

$$\delta\rho = -\frac{1}{\pi}\mathrm{Im\,Tr}\,\left[g^2\,V\,(1-gV)^{-1}\right] = \frac{1}{\pi}\mathrm{Im\,Tr}\,\left[\frac{\partial g}{\partial\omega}\,V\,(1-gV)^{-1}\right] = -\frac{\partial}{\partial\omega}\,\frac{1}{\pi}\mathrm{Im\,Tr\,Log}\,(1-gV)\,. \tag{C3}$$

We substitute Eq. (C3) in Eq. (C1) integrate by parts and obtain

$$U = \frac{1}{\pi}\int_{-\infty}^{0} d\omega\,\mathrm{Im\,Tr\,Log}\,(1-gV)\,. \tag{C4}$$

For two impurities, the expression within a logarithm is a 2-by-2 matrix

$$1 - gV = \begin{pmatrix}1 & 0\\ 0 & 1\end{pmatrix} - \begin{pmatrix}g_{11} & g_{12}\\ g_{21} & g_{22}\end{pmatrix}\begin{pmatrix}V_1 & 0\\ 0 & V_2\end{pmatrix}, \tag{C5}$$

where V_1 and V_2 describe the perturbations due to individual impurities. Equation (C5) can be conveniently reexpressed via the on-site T-matrices.

$$1 - gV = \begin{pmatrix}1-g_{11}V_1 & 0\\ 0 & 1-g_{22}V_2\end{pmatrix}\begin{pmatrix}1 & -g_{12}T_2\\ -g_{21}T_1 & 1\end{pmatrix},\ \text{where } T_i = V_i\,(1-g_{ii}V_i)^{-1}. \tag{C6}$$

We substitute the product (C6) in Eq. (C4) and find that the energy splits into two contributions $U = U_{\rm self} + U_{\rm int}$

$$U_{\rm self} = \frac{1}{\pi}\int_{-\infty}^{0} d\omega\,\mathrm{Im\,Tr\,Log}\begin{pmatrix}1-g_{11}V_1 & 0\\ 0 & 1-g_{22}V_2\end{pmatrix}, \qquad U_{\rm int} = \frac{1}{\pi}\int_{-\infty}^{0} d\omega\,\mathrm{Im\,Tr\,Log}\begin{pmatrix}1 & -g_{12}T_2\\ -g_{21}T_1 & 1\end{pmatrix}. \tag{C7}$$

The first contribution $U_{\rm self}$ gives the self-energy of the individual impurities, whereas the second contribution $U_{\rm int}$ describes the interaction between impurities and vanishes for large separation between impurititesi where $g_{12} \to 0$. Further, we simplify the logarithm in the expression for the interaction energy

$$\mathrm{Tr\,Log} \begin{pmatrix} 1 & -g_{12}T_2 \\ -g_{21}T_1 & 1 \end{pmatrix} = \mathrm{Log\,Det} \begin{pmatrix} 1 & -g_{12}T_2 \\ -g_{21}T_1 & 1 \end{pmatrix} = \mathrm{Log\,Det}\ (1 - g_{12}T_2 g_{21}T_1) \tag{C8}$$

where the property of determinants of Bloch matrices was used in the last equation. So, finally we obtain

$$U_{\rm int} = \frac{1}{\pi} \int_{-\infty}^{0} d\omega\ \mathrm{Im\,Tr\,Log}\ (1 - g_{12}T_2 g_{21}T_1)\,, \tag{C9}$$

where trace is now taken only in the space of indices of the Green's function.